Parallel Interacting Multiple Model-Based Human Motion Prediction for Motion Planning of Companion Robots

Donghan Lee, Chang Liu, *Student Member, IEEE*, Yi-Wen Liao, and J. Karl Hedrick

***Abstract*— We propose in this paper an autonomous motion planning framework for companion robots to accompany humans in a socially desirable manner, which takes safety and comfort requirements into account. The overall framework consists of two parts: first, a novel parallel interacting multiple model-unscented Kalman filter (PIMM-UKF) approach is developed to simultaneously estimate human motion states and model mismatch, and then systematically predict the position and velocity of the human for a finite horizon. Second, based on the predicted human states, a nonlinear model predictive control (MPC) technique is utilized for the robot motion planning. The simulation results have demonstrated the superior performance in prediction using the PIMM-UKF approach. The effectiveness of the MPC planner is also shown by successfully facilitating the socially desirable companion behavior.**

***Note to Practitioners*—This paper is motivated by the problem of allowing robots to autonomously accompany humans in search-and-rescue situations for providing assistance. For example, companion robots can carry heavy loads and follow human rescuers who want to search for survivors. Two types of requirements need to be taken into account for companion robots to achieve the so-called *socially desirable* companion behavior: first, the *safety* requirement requires robots strictly keep a safe distance from humans to avoid colliding and hurting people; second, it is desirable for robots to stay within a "comfort zone" around the human, and also maintain a similar speed to make human feel comfortable. This is referred as the *comfort* requirement. In order to generate socially desirable companion behavior, we specifically tackle two challenges in this paper: human motion prediction and robot motion planning. We propose an online prediction approach that simultaneously considers multiple typical human motion models to reflect natural movements of humans. In addition, we design a model mismatch estimator to compensate for the errors arising from the model uncertainty. Based on the predicted human motion, we use an optimal control-based approach to compute robot trajectories that satisfy the safety and comfort requirements. Ten randomly selected scenarios are used to evaluate the effectiveness of the proposed approach. The results show superior performance in terms of the accuracy and response time in the estimation and prediction using the proposed approach. Moreover, the motion planner successfully ensures *socially desirable* companion behavior. In the future work, we will investigate different learning-based approaches to estimate human motion in real time.**

***Index Terms*— Companion robots, interacting multiple model (IMM), model mismatch, model predictive control (MPC), motion planning, motion prediction, unscented Kalman filter (UKF).**

I. Introduction

THERE has been an increasing interest in developing and improving autonomous robots for search-and-rescue (SAR) missions in recent decades [1]–[5]. In years, human-companion robots have also received considerable attention [6]–[8]. One interesting intersection of these two fields is enabling intelligent robots to autonomously accompany human rescuers during SAR missions, carrying heavy apparatuses, detecting survivor signals, or exploring dangerous areas. A *socially desirable* companion robot is expected to behave in a safe and comfortable manner when accompanying a person [6], [9]. The safety concern addressed here requires that the robot avoid collisions that could hurt humans or the robot itself [10]. The comfort requires robots to pose little annoyance and stress for the human [9], which is mainly focused on the *human spatial behavior* [11] and is usually formulated in terms of the distance between the robot and the humans. It has also been considered as a contributing factor to comfort if the robot maintains a similar speed as the human [12].

Accurate human motion prediction is vital for generating robot's socially desirable motion behavior. To be specific, the robot needs to predict human future trajectories based on human's motion states that are obtained from measurement tools, such as GPS sensors or cameras. Filtering methods, such as Kalman filters (KFs) and particle filters (PFs), have commonly been applied for predicting and tracking moving objects [13]–[15]. These model-based filtering approaches can effectively predict human motion when people's motion can be accurately captured by the model used in the filters, such as the constant speed and direction model [8], [10]. However, when the human movement consists of multiple motion patterns, such as making turns, moving in curvature and changing speed, such methods may fail to give an accurate prediction.

Learning techniques have also been utilized for human motion prediction in recent years. For example, Fulgenzi *et al.* [16] developed a Gaussian process-based

Manuscript received August 18, 2016; accepted October 23, 2016. Date of publication December 2, 2016; date of current version January 4, 2017. This paper was recommended for publication by Editor Y. Sun upon evaluation of the reviewers' comments.

D. Lee, C. Liu, and Y.-W. Liao are with the Vehicle Dynamics and Control Laboratory, Department of Mechanical Engineering, University of California at Berkeley, Berkeley, CA 94720 USA (e-mail: donghan.lee@berkeley.edu; changliu1289@gmail.com; ywliao@berkeley.edu).

J. K. Hedrick is with the Department of Mechanical Engineering, University of California at Berkeley, Berkeley, CA 94720 USA (e-mail: khedrick@me.berkeley.edu).

Color versions of one or more of the figures in this paper are available online at http://ieeexplore.ieee.org.

Digital Object Identifier 10.1109/TASE.2016.2623599

motion predictor using prelearned human motion patterns. Trautman *et al.* [17] proposed an interactive Gaussian process approach for predicting human motion, considering their interaction with the robot. Human dynamics were modeled as the mixture of different kernels. Xiao *et al.* [18] predicted human future trajectory by classifying the observed human motion into homogeneous motion classes, using pretrained support vector machine. These learning-based approaches have achieved success in predicting human motion in the environments, where human trajectories have been previously collected for training. However, they may fail to obtain accurate prediction in unknown environments for which no training data are available. This drawback renders the learning-based prediction methods less applicable for SAR missions, since disaster sites are diverse and rarely similar to the known ones.

In this paper, we propose a parallel interacting multiple model-unscented KF (PIMM-UKF) approach for human motion estimation and prediction, taking advantage of the fact that human motion usually consists of different motion patterns [19]. The IMM approach incorporates several typical motion models and dynamically adjusts the mode probabilities based on the observed human trajectory [20]. To deal with the nonlinearity of the human motion, such as making turns, a UKF is applied to each model in the IMM framework, resulting in the so-called IMM-UKF structure [21]. In order to account for the effects of unmodeled dynamics of a human, we design a model mismatch estimator that augments the IMM-UKF structure, which further improves the prediction of human motion. Two independent IMM-UKF estimators are thus used in tandem to estimate states and model mismatch simultaneously, and then systematically predict the future motion of the human, which forms the PIMM-UKF approach. Such method can achieve higher prediction accuracy and faster response compared with single-model filtering methods, such as KF and PF. In addition, PIMM-UKF does not require training and is thus applicable to unknown environments, which is advantageous over learning-based methods for SAR missions.

Utilizing the predicted human trajectory, a nonlinear model predictive control (MPC)-based motion planner [22] is developed that formulates the motion planning as a finite-horizon constrained optimal control problem (FHCOCP), which conveniently considers the safety and comfort requirements. The autonomous motion planning system consisting of the MPC planner with PIMM-UKF predictor is then evaluated using ten randomly generated SAR scenarios in simulations, in which the human rescuer moves sequentially to several destinations and the robot autonomously accompanies. Simulation results show that the PIMM-UKF approach provides superior prediction performance than IMM-UKF and single-model-based UKF. With the MPC motion planner, the robot successfully accompanies the human in a safe and comfortable manner.

The remainder of this paper is organized as follows. First, the problem of motion planning for a human-companion robot in the SAR mission is formulated in Section II. Then, the overall architecture of the motion planning system, including the PIMM-UKF-based human motion prediction and MPC-based motion planner, is described in Section III. The simulation setup and the results on evaluating the proposed approach are presented in Section IV. This paper is concluded with the ideas of future work in Section V.

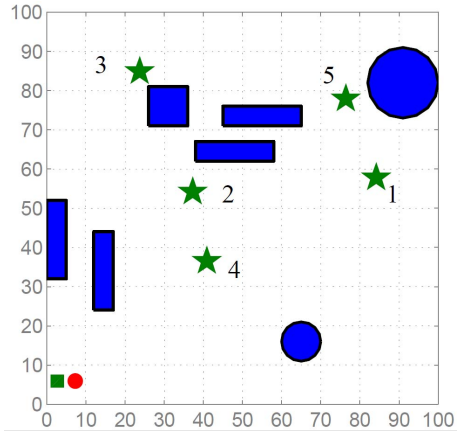

Fig. 1. SAR scenario for the companion robot to accompany a human. The red circle and the green square represent the human rescuer and the robot companion, respectively. There are five randomly generated target positions (green stars) that the human should arrive sequentially (in the ascending order of the numbers next to each target position). Blue shapes represent the obstacles.

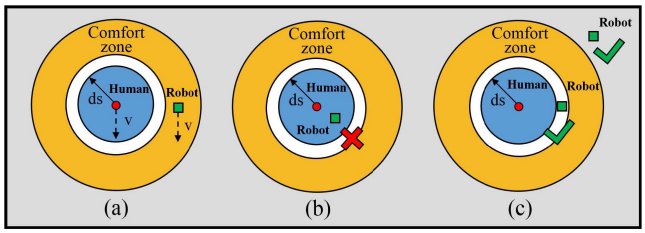

Fig. 2. Illustration of safety and comfort requirements. (a) Most desirable companion behavior is that the robot stays within the "comfort zone" and maintains similar speed as the human. (b) Robot is not allowed to enter the "unsafety zone." (c) It is acceptable that the robot stays outside the "comfort zone" and the "unsafety zone."

II. Problem Formulation

Consider an example of SAR scenarios in 2-D space (Fig. 1), in which a human first responder needs to deliver medical treatment to several destinations that have injured people. A companion robot that carries medical apparatus will accompany the human in a socially desirable way, and sequentially move to these destinations. The robot has no prior knowledge about the human destinations. However, it can measure human positions in real time from the measurement tools, such as GPS sensors or cameras. Neither the robot nor human can enter or traverse obstacles, represented by blue polygons and circles. The position and the dimension of obstacles are provided by satellite maps or aerial images.

When accompanying the human, the robot is expected to obey the aforementioned safety and comfort requirements, as shown in Fig. 2. To be specific, a circular "unsafety zone" (blue circle) with radius d_s is defined around the target person. Stepping into the "unsafety zone" is considered as risky behavior, and thus should be strictly prohibited.

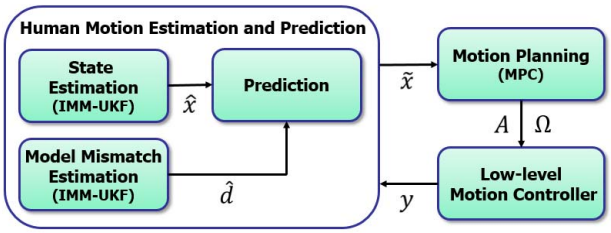

Fig. 3. Diagram of the overall system of the companion robot.

The comfort requires the robot to stay within a "comfort zone" (orange area) around the human, and also keep similar speed. We adopt the "Proxemics" model, proposed by Hall *et al.* [23], for designing the "comfort zone" in the way similar to works on human–robot interaction [7], [24]. Comfort is a soft requirement in that a robot may move outside of the "comfort zone" [Fig. 2(c)], though not desirable.

III. Methods

A. System Description

The proposed system architecture is shown in Fig. 3. The system consists of two intertwined components: the module for human motion estimation and prediction and the module for robot motion planning. For the former, we propose a parallel-estimation structure, denoted as the "state estimation" block and the "model mismatch estimation" block in Fig. 3, for estimating human motion states and the model mismatch, respectively. These estimates are then used for probabilistic prediction of human motion in the near future. The "motion planning" block utilizes the forecast evolution of human motion states to design the robot companion behavior via optimizing the acceleration and the orientation of the robot under the MPC framework. We assume that the robot can measure the longitudinal and the lateral position of the human using sensors, such as GPS or cameras.

B. Human Motion Estimation and Prediction

1) Interacting Multiple Model: The IMM approach is usually applied for estimating the system states from noisy sensor data. It utilizes a bank of r number of filters, each corresponding to a different motion model. State estimate at time k is computed as a weighted sum of estimates from each filter, as shown in the following formula:

$$\hat{x}_{k|k} = \sum_{j=1}^{r} \mu_{j,k} \hat{x}^{j}_{k|k} \tag{1}$$

where $\hat{x}^{j}_{k|k}$ represents the state estimate from the jth filter and $\hat{x}_{k|k}$ is the overall state estimate; $\mu_{j,k}$ stands for the mode probability and can be recursively computed as follows:

$$\mu_{j,k} = \frac{1}{c} \sum_{i=1}^{r} L_{ij,k}\, p_{ij}\, \mu_{j,k-1}$$

where $L_{ij,k}$ stands for the Gaussian likelihood of receiving the current measurement given all previous measurements and that the jth model is in effect at time k; p_{ij} represents the mode transition probability from the ith to the jth model; c denotes the normalizing factor. Each filter uses the mixed initial state estimate and covariance from an interaction of the r filters, which consists of the combination of the estimates with the mixing probability at previous time step. Readers interested in the details of the IMM approach can refer to [20].

In this paper, two different kinematic models are used in the IMM framework: one for the coordinated turn motion model, reflecting the action of making turns or moving along a curved path, and the other for the uniform motion model, representing the constant heading movement.

The equation for the coordinated turn motion model is shown below

$$x^{h,1}_{s,k+1} = f^1_s\big(x^{h,1}_{s,k}\big) + G_s w_{1,k} \tag{2a}$$

$$f^1_s\big(x^{h,1}_{s,k}\big) = \begin{bmatrix} p^h_1 + \dfrac{\sin(\omega^h T)}{\omega^h} v^h_1 - \dfrac{1-\cos(\omega^h T)}{\omega^h} v^h_2 \\ \cos(\omega^h T) v^h_1 - \sin(\omega^h T) v^h_2 \\ p^h_2 + \dfrac{1-\cos(\omega^h T)}{\omega^h} v^h_1 + \dfrac{\sin(\omega^h T)}{\omega^h} v^h_2 \\ \sin(\omega^h T) v^h_1 + \cos(\omega^h T) v^h_2 \\ \omega^h \end{bmatrix} \tag{2b}$$

$$G_s = \begin{bmatrix} \dfrac{T^2}{2} & 0 & 0 \\ T & 0 & 0 \\ 0 & \dfrac{T^2}{2} & 0 \\ 0 & T & 0 \\ 0 & 0 & 1 \end{bmatrix} \tag{2c}$$

$$w_1 \sim \mathcal{N}\big(0, Q^1_s\big) \tag{2d}$$

and the equation of the uniform motion model is represented as follows:

$$x^{h,2}_{s,k+1} = f^2_s\big(x^{h,2}_{s,k}\big) + G_s w_{2,k} \tag{3a}$$

$$f^2_s\big(x^{h,2}_{s,k}\big) = \begin{bmatrix} p^h_1 + v^h_1 T \\ v^h_1 \\ p^h_2 + v^h_2 T \\ v^h_2 \\ 0 \end{bmatrix} \tag{3b}$$

$$w_2 \sim \mathcal{N}(0, Q^2_s) \tag{3c}$$

where $x^{h,i}_{s,k}$, $i = 1, 2$ represents the human motion state, including five elements: $[p^h_1, v^h_1, p^h_2, v^h_2, \omega^h]^T$,[1] where p^h_1 and p^h_2 denote the longitudinal and lateral positions, v^h_1 and v^h_2 the corresponding velocity, and ω^h the turn rate; T is the sampling time; $w_{i,k}$, $i = 1, 2$ represents the process noise that follows a zero-mean Gaussian distribution with Q^i_s being the covariance matrix.

The uniform motion model is essentially a special case of the coordinated turn motion model with the turn rate ω being fixed to zero. It seems that only considering the coordinated turn motion model suffices to estimate human motion states, in addition to the benefits of reduced computations by using the single model. However, including two models are necessary, since this allows the estimator for fast detection of change of motions, which is shown in [25].

[1]We omit k and i in the notation for the purpose of notational simplicity.

The sensor observation model is represented as

$$y_{s,k}^{h,i} = C_s x_{s,k}^{h,i} + v_k \tag{4}$$

where $y_{s,k}^{h,i}$ denotes the observed human state at time step k; v_k stands for measurement noise. By using GPS or camera sensors, the human positions can be directly measured. Therefore, the parameters in observation model (4) are defined as

$$C_s = \begin{bmatrix} 1 & 0 & 0 & 0 & 0 \\ 0 & 0 & 1 & 0 & 0 \end{bmatrix}, \quad v_k \sim \mathcal{N}(0, V_s)$$

where V_s is the covariance matrix of the measurement noise. Note that $y_{s,k}^{h,1}$ and $y_{s,k}^{h,2}$ are equivalent to the actual measurement.

2) Unscented Kalman Filter: The UKF is applied to each motion model that is used in IMM framework for estimating human states. It is an effective state estimation technique for nonlinear systems by implementing the unscented transformation that calculates the statistics of a random vector that undergoes a nonlinear transformation [26]. To be specific, given an arbitrary nonlinear motion model $z = g(x)$ and an L-dimensional Gaussian random vector x with mean $\hat{x}$ and covariance P_x, the statistics of z can be approximated by using $2L+1$ discrete sample points $\{\chi^{(i)}\}_{i=0}^{2L} = \{\hat{x} \text{ and } \hat{x} \pm \sigma_j,\ j = 1, \ldots, L\}$, called *sigma points*, where σ_j is the jth column of the matrix $((L+\lambda)P_x)^{1/2}$. $\lambda = \alpha^2(L+\kappa) - L$ is a scaling parameter [27].

Once the sigma points have been generated, each point is passed through the nonlinear function $z = g(x)$, i.e., each column of the sigma points is propagated through the nonlinearity, as in $\zeta^{(i)} = g(\chi^{(i)}), i = 0, \ldots, 2L$. The mean $\hat{z}$ and the covariance P_z are approximated as $\hat{z} \simeq \Sigma_{i=0}^{2L} W_i^{(m)} \zeta^{(i)}$ and $P_z \simeq \Sigma_{i=0}^{2L} W_i^{(c)} (\zeta^{(i)} - \hat{z})(\zeta^{(i)} - \hat{z})^{\mathsf{T}}$, with weights and parameters calculated in

$$W_0^{(m)} = \frac{\lambda}{L+\lambda} \tag{5a}$$

$$W_0^{(c)} = \frac{\lambda}{L+\lambda} + 1 - \alpha^2 + \beta \tag{5b}$$

$$W_i^{(m)} = W_i^{(c)} = \frac{1}{L+\lambda}, \quad i = 1, \ldots, 2L \tag{5c}$$

where α determines the spread of sigma points about the mean $\hat{x}$; κ is a secondary scaling parameter; β is used to incorporate prior knowledge of the distribution. The state estimate, $\hat{x}_{k|k}^{j}$, $j = 1, \ldots, r$ in (1) can be computed like $\hat{z}$ here at each filter that corresponds to a different motion model. Readers can refer to [26] and [28] for more details of the UKF algorithm.

3) Model Mismatch Estimation: A model mismatch estimation algorithm that is able to capture unmodeled dynamics of humans is proposed for the purpose of improving human motion prediction. The augmented state formulation is one of the most popular approaches used to compensate for model-plant mismatch [29]–[31]. The model mismatch estimator is obtained by appending each motion model in IMM-UKF with three additional states, corresponding to the mismatch of longitudinal position, lateral position, and turn rate. By applying IMM-UKF to the augmented system, each additional state can be estimated online, and then added to the predicted human positions, velocities, and turn rates as corrective terms. This process corresponds to the "human motion estimation and prediction" component in Fig. 3.

At the first sight, it seems that merely using the augmented IMM-UKF estimator is sufficient for estimating both states and model mismatch. However, it is necessary to maintain two separate estimators that correspond to the state estimator and the model mismatch estimator, which stems from the tradeoff between two main concerns in designing estimators: the fast response and the noise rejection. In this paper, the model mismatch estimator needs to track human trajectories as fast as possible to precisely measure model mismatch so as to compensate for the inaccurate prediction of the human motion. However, the requirement of fast tracking usually results in very noisy human state estimation, which is not suitable for reliable prediction. Thus, we propose the parallel IMM-UKF framework to simultaneously produce the estimates of states and model mismatch. The state estimation IMM-UKF is designed to reject the noise from observations with slower tracking response than the model mismatch estimation. The model mismatch estimation IMM-UKF, on the other hand, is designed to achieve fast tracking of human motion states even if the state estimation results are noisy. This is achieved by setting a large process noise for the additional three states while keeping the process noise for the original states the same as the ones used in the state estimator. The coordinated turn motion and uniform motion models for the model mismatch estimation are shown in Appendix A.

4) Human Motion Prediction: The PIMM-UKF is then used for predicting human motion, incorporating the estimated human motion states and model mismatch. To be specific, using the uniform motion model and the turn motion model, human positions and velocities in each model can be extrapolated based on the current estimated state and model mismatch. Prediction from each model is then combined according to the mode probabilities to obtain the overall predicted human motion state. Let $\hat{x}_{k|k}^{h,j}$, $\tilde{x}_{k+i|k}^{h,j}$, and $\hat{d}_{k|k}^{h,j}$ represent the estimated and predicted human states and the estimated model mismatch associated with the jth model at time k and $k+i$ $(i \geq 0)$, respectively, based on the observations up to time k. The prediction procedure works as follows:

$$\tilde{x}_{s,k+l+1|k}^{h} = \sum_{j=1}^{r} \mu_j \tilde{x}_{s,k+l+1|k}^{h,j} \tag{6a}$$

$$\tilde{x}_{s,k+l+1|k}^{h,j} = f_s^j\left(\tilde{x}_{s,k+l|k}^{h,j}\right) + h_s^j\left(\hat{d}_{k|k}^{h,j}\right) \quad l = 0, \ldots, N-1 \tag{6b}$$

$$\tilde{x}_{s,k|k}^{h,j} = \hat{x}_{s,k|k}^{h,j}, \quad j = 1, \ldots, r$$

$$h_s^j\left(\hat{d}_{k|k}^{h,j}\right) = \begin{bmatrix} \frac{T^2}{2}\hat{d}_1^{h,j} \\ T\hat{d}_1^{h,j} \\ \frac{T^2}{2}\hat{d}_2^{h,j} \\ T\hat{d}_2^{h,j} \\ T\hat{d}_3^{h,j} \end{bmatrix} \tag{6c}$$

where N denotes the prediction horizon; r is the number of models. f_s^j represents each model in (2) and (3).

C. Robot Motion Planning

1) Model Predictive Control: The MPC approach is utilized for robot motion planning. MPC is an advanced optimal control approach to iteratively generate control inputs for constrained dynamical systems. At each time step, MPC computes the optimal control inputs by solving an FHCOCP, taking into account the system evolution in the planning horizon; however, only the control input for the current time step is implemented to the system. At the next time step, FHCOCP is solved again based on the updated system states.

2) Kinematics Model of Companion Robot: One desirable candidate for SAR applications is the wheeled mobile robot. Its kinematics model can be described by a nonlinear unicycle model. The following difference equations are obtained by the forward Euler discretization with the sampling time T:

$$x^r_{k+1} = f_r\left(x^r_k\right)$$
$$f_r(x^r_k) = \begin{bmatrix} p^r_{1,k} + v^r_k \cos\theta^r_k T \\ p^r_{2,k} + v^r_k \sin\theta^r_k T \\ v^r_k + a^r_k T \\ \theta^r_k + \omega^r_k T \end{bmatrix} \tag{7}$$

where the state $x^r_k = [p^r_1, p^r_2, v^r, \theta^r]^T$ consists of the robot's xy-positions, velocity, and yaw angle. The acceleration a^r_k and the yaw rate ω^r_k are the control inputs. For simplicity, we define the position vector $p^r_k = [p^r_1, p^r_2]^T$.

3) Controller Design: To design the MPC controller, we first obtain the estimated and predicted human states, $\tilde{x}^h_{s,k+i|k}$ for horizon $i = 0 \ldots N$ at time step k from PIMM-UKF according to (6). The state contains five elements, which are $[\tilde{p}^h_1,\ \tilde{v}^h_1,\ \tilde{p}^h_2,\ \tilde{v}^h_2,\ \tilde{\omega}^h]^T$. Calculate the tracking reference of the human position vector and velocity as follows:

$$\tilde{p}^h_{k+i|k} = \begin{bmatrix} \tilde{p}^h_{1,k+i|k} \\ \tilde{p}^h_{2,k+i|k} \end{bmatrix}, \quad i = 0 \ldots N$$
$$\tilde{v}^h_{k+i|k} = \left\| \begin{bmatrix} \tilde{v}^h_{1,k+i|k} \\ \tilde{v}^h_{2,k+i|k} \end{bmatrix} \right\|_2, \quad i = 0 \ldots N.$$

Then, we can obtain the current optimal control input at time step k by solving the following FHCOCP that incorporates the kinematics of the robot (7) and the safety and comfort requirements:

$$\min_{\mathbf{A}_k, \Omega_k} \sum_{i=0}^{N} q_1 \left| \left\| p^r_{k+i|k} - \tilde{p}^h_{k+i|k} \right\|_2^2 - d_c^2 \right| + q_2 \left(v^r_{k+i|k} - \tilde{v}^h_{k+i|k}\right)^2 + q_3 \left({a^r_{k+i|k}}^2 + {\omega^r_{k+i|k}}^2\right) \tag{8a}$$
$$\text{s.t. } x^r_{k+i+1|k} = f_r\left(x^r_{k+i|k}\right) \tag{8b}$$
$$a_{lb} \le a^r_{k+i|k} \le a_{ub}, \quad w_{lb} \le \bar{\omega}^r_{k+i|k} \le w_{ub} \quad i = 0, \ldots, N-1 \tag{8c}$$
$$\left\| p^r_{k+i|k} - \tilde{p}^h_{k+i|k} \right\|_2 > d_s, \quad i = 0, \ldots, N \tag{8d}$$
$$h_{l_s}\left(p^r_{k+i|k}\right) > 0, \quad l_s = 1, \ldots, n_s \tag{8e}$$
$$p^r_{k|k} = p^r_k, \quad v^r_{k|k} = v^r_k, \quad \theta^r_{k|k} = \theta^r_k \tag{8f}$$

where $p^r_{k+i|k}$, $v^r_{k+i|k}$, and $\theta_{k+i|k}$ for $i = 1 \ldots N$ represent the planned position, velocity, and heading angle of the robot at time $k+i$; n_s is the number of obstacles. The obstacles are approximated by ellipses, and $h_{l_s}(\cdot)$ denotes the analytical function of the ellipse approximation of the l_sth obstacle. The details of which are described in Appendix B.

The objective function (8a) consists of three terms: the first one stands for the difference between the squared human–robot distances and the squared comfort distance d_c, which could take any value within the "comfort zone"; the second one represents the velocity difference between the robot and the human. These reflect the comfort requirement that the robot stay within the "comfort zone" around the human, and keep similar pace at the same time. Finally, the last term penalizes the control inputs. q_1, q_2, and q_3 denote the positive weights for these three terms. The robot kinematics (8b) are defined in (7), with (8c) being the upper and lower bounds for the control inputs. The safety constraints are imposed in (8d) that requires the robot stay at least the safety distance d_s from the human in order to avoid collision. Equation (8e) enforces the collision avoidance with obstacles by demanding that, at each prediction step, the robot should not intersect with obstacles. Equation (8f) initializes the robot's planned states based on its state at time k.

The solution of the optimal control input, $(\mathbf{A}^*_k, \mathbf{\Omega}^*_k)$, consists of the sequence of optimal acceleration $a^{r*}_{k+i|k}$ and angular velocity $\omega^{r*}_{k+i|k}$ of the robot in the prediction horizon $i = 0 \ldots N-1$. To reduce the formulation complexity of the FHCOCP, we first solve the problem without the obstacle constraints (8e). After obtaining the optimal solutions, $(\mathbf{A}^*_k, \mathbf{\Omega}^*_k)$, we check if the predicted positions violate any obstacle constraint. If violation happens, FHCOCP at time k is recomputed with the corresponding obstacle constraints being activated. When there is no obstacle constraint violation, $a^{r*}_{k|k}$ and $\omega^{r*}_{k|k}$ are implemented as the robot's control input.

IV. Simulation Results and Discussion

A. Simulation Setup

The proposed motion planner for human-companion robots is evaluated in ten randomly generated SAR scenarios, each with the size of 100 m $\times$ 100 m. Five destinations that the human rescuer needs to move to sequentially were randomly chosen. In each scenario, there were seven obstacles with polygon or circular shapes and of different sizes. They were randomly placed in the way that no obstacle overlapped. The trajectory of the human rescuer was generated by the RRT algorithm [32], with speed randomly varying from 1 to 1.5 m/s. The RRT algorithm realistically simulated human-like motion trajectories that included straight-line motion, curved motion, change of speeds, and making abrupt turns. One of the scenarios is shown in Fig. 4(a), with human trajectory represented by the red broken line. The safety distance d_s was set to be 1 m. According to the research conducted by Hall *et al.* [23], the comfort distance ranges from 1.2 to 3.6 m. In the simulation, d_c was chosen as 2.8 m, and any distance within [1.2, 3.6 m] was considered a comfortable one. The GPS sensor or camera sensor for locating the human rescuer had a sampling rate of 20 Hz. The robot's maximum acceleration and deceleration were set to be 1 and -3 m/s^2, respectively, and the angular velocity range was chosen to be [$-90°$/s, $90°$/s]. The process noise and measurement noise

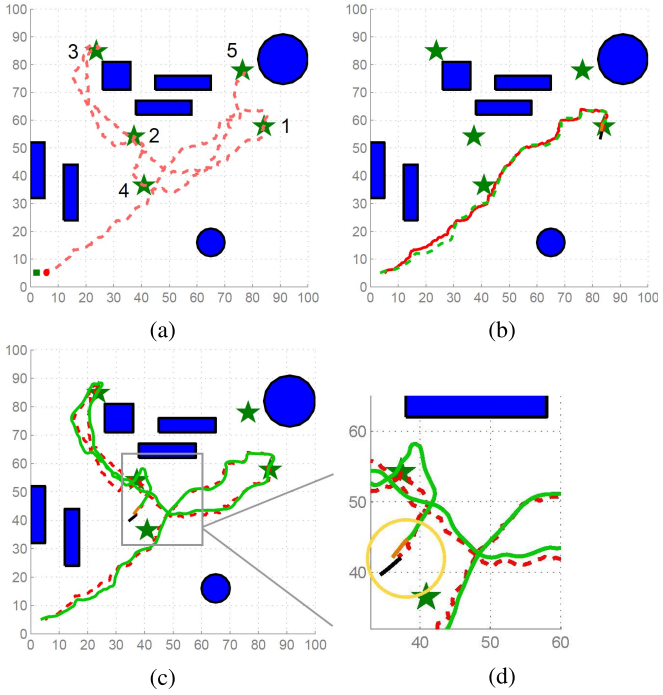

Fig. 4. Screenshot of the simulation. (a) Red broken line represents the human trajectory and the green solid line shows the companion robot's trajectory. (b) Both human and robot arrive at the first target. (c) Human is heading to fourth target. (d) Black line shows the predicted trajectory of the human from PIMM-UKF and the brown line shows the planned trajectory of the robot using MPC.

for the IMM estimator were set to be 1.5×10^{-2} and 1.5, respectively. The parameters of UKF in the estimator were $L = 5$, $\alpha = 0.001$, $\kappa = 0$, and $\beta = 2$. The prediction horizon for the human motion was 2.5 s and the robot iteratively computed the control inputs every 500 ms.

B. Simulation Results

Fig. 4(a)–(d) shows both the human and robot's trajectories for one of the ten scenarios. The performance of human motion estimation is first evaluated by comparing IMM-UKF with each single-model-based UKF. The performance of PIMM-UKF is then compared with IMM-UKF for human motion prediction. The MPC-based robot motion planning method is then evaluated under two different cases: one with the prediction and other without the prediction.

1) Human Motion Estimation: The error between the estimated and the actual human position and velocity at each time step is compared to evaluate the accuracy of the estimation. The position error vector is defined as

$$\Delta_p^{\text{est}}(k) = p_k^h - \hat{p}_{k|k}^h$$

where p_k^h denotes the actual human position at time k.

Fig. 5 shows the root-mean-square (rms) errors of the estimated positions on longitudinal and lateral directions using three different estimators: uniform motion model-based UKF, turn motion model-based UKF, and IMM-UKF. It is easy to notice that IMM-UKF achieves smaller rms position errors than both single-model-based UKFs. IMM-UKF generates more accurate estimation when the human suddenly changes the motion, such as at time 200 and 250, in particular.

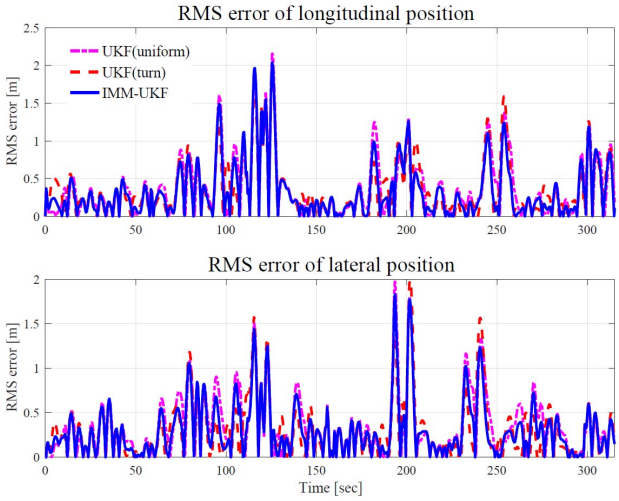

Fig. 5. Comparison of rms errors estimated position with each single-model-based UKF and IMM-UKF.

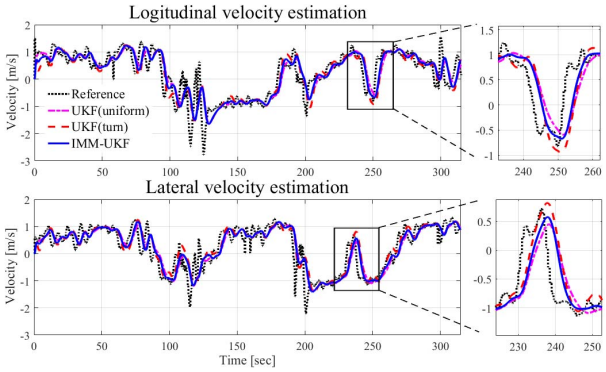

Fig. 6. Comparison of the estimated velocity using each single-model-based UKF and IMM-UKF.

TABLE I
RMS ERROR OF THE ESTIMATED POSITION AND VELOCITY

	Direction	UKF(uniform)		UKF(turn)		IMM-UKF	
		mean	std.	mean	std.	mean	std.
Position [m]	Long.	0.52	0.04	0.48	0.02	0.46	0.03
	Lat.	0.51	0.05	0.46	0.05	0.46	0.05
Velocity [m/s]	Long.	0.59	0.03	0.60	0.02	0.58	0.02
	Lat.	0.57	0.03	0.57	0.03	0.56	0.03

Fig. 6 compares the velocity estimation using the three different estimators. Overall, the IMM-UKF estimator shows the faster response than the uniform motion model-based UKF, though with the tradeoff of small overshoot. When compared with the turn motion model-based UKF, as shown in the enlarged plots, IMM-UKF achieves smaller overshoots and faster convergence to the true velocity. This makes sense as the IMM-UKF estimator incorporates uniform motion model that can capture the sudden velocity changes.

The average and the standard deviation of the rms errors of the estimated position and velocity for the ten randomly generated scenarios are compared in Table I. IMM-UKF achieves smaller than each single model-based-UKF, which shows that IMM-UKF provides improved position and velocity estimation in both directions.

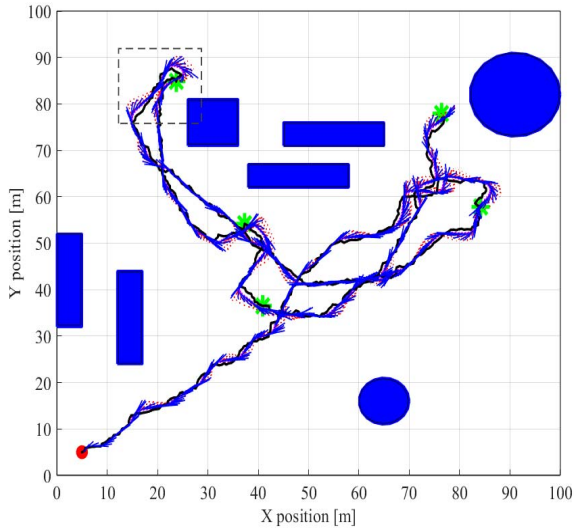

Fig. 7. Illustration of the human motion prediction.

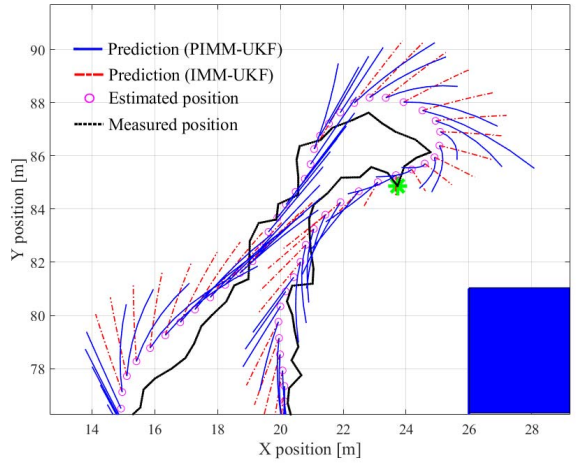

Fig. 8. Comparison of the human motion prediction using IMM-UKF and PIMM-UKF.

2) Human Motion Prediction: Fig. 7 shows the human motion prediction for the scenario in Fig. 4(a). The enlarged figure of the top-left corner is shown in Fig. 8. Black solid line represents the measurements from sensors, and pink color circles show the estimated positions. Five-step predicted positions are shown as two types of line: red broken lines represent the prediction from IMM-UKF and blue solid lines stand for the results from PIMM-UKF, taking model mismatch estimation into account. It is obvious that the prediction with the model mismatch estimation is much closer to the actual human motion states than the other, which shows that incorporating model mismatch estimator into the prediction process significantly improves human motion prediction.

To quantitatively evaluate the prediction of different approaches, we first compare the prediction errors over the prediction horizon between single-model-based UKFs and IMM-UKF; then, we subsequently compare the metrics between PIMM-UKF and IMM-UKF. At time k, the prediction

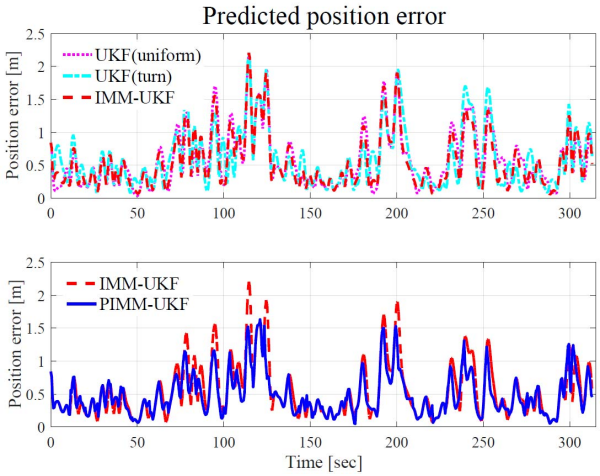

Fig. 9. Comparison of predicted position error using each single-model-based UKF, IMM-UKF, and PIMM-UKF.

TABLE II
ERROR OF THE PREDICTED POSITION AND VELOCITY

	Direction	IMM-UKF		PIMM-UKF	
		mean	std.	mean	std.
Position [m]	Long.	0.37	0.32	0.34	0.26
	Lat.	0.36	0.32	0.32	0.25
Velocity [m/s]	Long.	0.27	0.14	0.27	0.14
	Lat.	0.26	0.14	0.25	0.13

error is defined as

$$\Delta_{p,k}^{\text{pre}} = \frac{1}{N}\sum_{i=1}^{N} \left\| \tilde{p}_{k+i|k}^{h} - p_{k+i}^{h} \right\|_2.$$

Fig. 9 shows the comparison of predicted position errors using each single-model-based UKF, IMM-UKF, and PIMM-UKF. It can be noticed that each single-model-based UKF generates larger prediction error than IMM-UKF, especially when the human makes sharp turns, such as at time 120 and 240 in the top plot. Moreover, the bottom plot in Fig. 9 shows that PIMM-UKF outperforms IMM-UKF for most of the parts. For the ten randomly generated scenarios, Table II shows that the average errors of the position of PIMM-UKF are smaller than those of IMM-UKF, which demonstrates that the model mismatch estimation indeed improves the human motion prediction.

s

3) Robot Motion Planning: Fig. 4(d) shows the planned trajectory of the companion robot that accompanies the target person moving in the field. The trajectory is generated by the proposed MPC motion planner with five-step planning horizon (2.5 s) and using the proposed PIMM-UKF approach for predicting the human trajectories. The performance of the motion planning is evaluated using the criterion of safety and comfort. To be specific, the distance and velocity differences between the robot and the human at each time step are computed using

$$\Delta_{d,k} = \left\| p_k^r - p_k^h \right\|_2$$
$$\Delta_{v,k} = v_k^r - v_k^h.$$

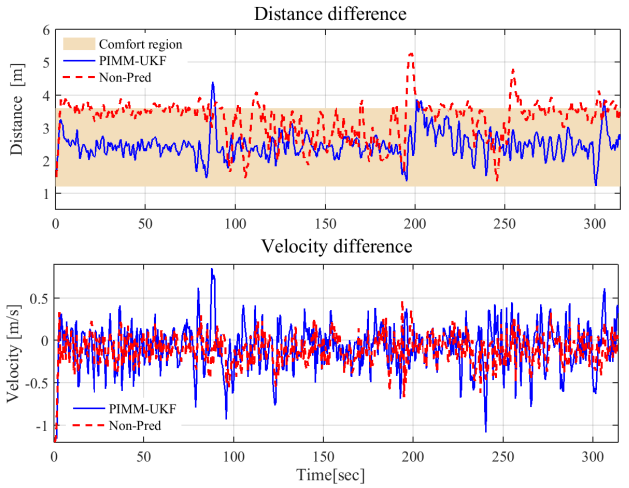

Fig. 10. Comparison of distance and velocity differences between the human and the robot.

TABLE III
PERFORMANCE OF TWO MPC-BASED MOTION PLANNERS

	PIMM-UKF prediction		Non-prediction	
	mean	std.	mean	std.
Distance diff. (m)	2.37	0.49	3.35	0.54
Velocity diff. (m/s)	-0.05	0.26	-0.12	0.20

The performance is compared with nonprediction case, in which the robot does not predict the human motion and only utilizes the human's current state as a reference to make a one-step horizon (0.5 s) motion planning.

Fig. 10 shows the comparison results of the distance and velocity differences between the human and the robot. We can see that the MPC planner is able to ensure the safety of the accompanied human with both two strategies for the selected scenario here: no distance between the human and the robot drops below the safety distance (1 m). However, it is worth noting that the nonprediction planner actually has a higher chance to violate the safety constraint, since it does not include the future prediction into the planning (see Fig. 11 for another scenario). In addition, by incorporating the human motion prediction via PIMM-UKF approach into the motion planning, the companion performance of the robot is significantly improved from the nonprediction case. As we can see, the robot can stay closer to the human while maintaining a comfortable distance almost all the time. With the prediction, the robot can also respond faster when the human suddenly changes the motion pattern (i.e., the sharp turns). In fact, we can see from Fig. 10 that the robot can catch up with the human easily compared with the nonprediction case around 200 and 250 s at the third and fourth targets.

Table III shows the mean and the standard deviation values of the distance and velocity differences between the human and the robot for the ten scenarios. Overall, smaller average distance and velocity differences (2.37 m and -0.05 m/s) can be achieved using the PIMM-UKF prediction approach, compared with the values of the nonprediction case (3.35 m and -0.12 m/s). Different from the out-performance in the mean values of the distance and velocity differences, the

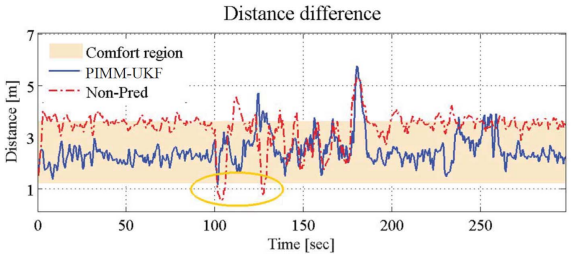

Fig. 11. Comparison of the distance difference between the human and the robot for another scenario.

PIMM-UKF prediction approach achieves a larger standard deviation in velocity difference (0.26 m/s) than the one in the nonprediction case (0.20 m/s). This seems to imply that the nonprediction method is preferable for the robot in the sense of keeping stable pace as the human. However, it should be noted that such velocity variance leads to large distances between the human and the robot that are out of the "comfort zone," as shown in Figs. 10 and 11, which is undesirable. In fact, the change of the velocity when using the prediction results from the motion planner's effort to keep the robot within the proximity of the human. Therefore, the simulation results show the effectiveness of the MPC motion planner and the benefits of incorporating the PIMM-UKF prediction into the planning process.

V. CONCLUSION

We have developed an autonomous motion planning framework for human-companion robots to accompany a target person in a socially desirable manner. Such companion robot can be useful for SAR scenarios by assisting humans in carrying apparatus, exploring dangerous areas or detecting survivors. A PIMM-UKF approach is proposed for the human motion prediction. It combines two independent IMM-UKF estimators to estimate the human motion states and model mismatch simultaneously. Both IMM-UKF estimators incorporate the uniform motion model and the coordinated turn motion model to allow the mixed system dynamics. Moreover, a corrective term provided by the model mismatch estimator is added into the human motion prediction. Such prediction framework captures different human motion patterns and the unmodeled dynamics, thus being able to obtain more accurate prediction. Based on the predicted results, the MPC is used to plan the robot's trajectory. Both the safety and comfort requirements are formulated into an FHCOCP.

The proposed motion planning framework is evaluated using ten randomly generated SAR scenarios in the simulations. The results show superior performance in terms of the accuracy and response time in the estimation and prediction using PIMM-UKF approach compared with IMM-UKF and each single-model-based-UKF methods, especially when the human makes curved motions or sharp turns. Moreover, the MPC planner is evaluated using the PIMM-UKF and nonprediction methods. The planner successfully ensures the safety of the accompanied person using these two prediction strategies, but the PIMM-UKF results in a better robot motion behavior by keeping the robot within the comfort zone from the human.

In the future work, we plan to compare other motion prediction methods, such as the autoregressive moving-average method, with PIMM-UKF approach. Besides, enabling the robot to learn human motion model in real time is an attractive topic, and may provide more accurate human motion prediction and results in better human-companion behavior.

APPENDIX

A. Model Mismatch Estimation

The IMM-UKF approach is extended to estimate the model mismatch to improve the prediction of the human motion. Two different augmented kinematic models containing model mismatch, as states are utilized in IMM framework. The coordinated turn motion model for the model mismatch estimation is shown in the following:

$$x_{d,k+1}^{h,1} = f_d^1\left(x_{d,k}^{h,1}\right) + G_d w_{1,k}$$

$$f_d\left(x_{d,k}^{h,1}\right) = \begin{bmatrix} p_1^h + \frac{\sin(\omega^h T)}{\omega^h} v_1^h - \frac{1-\cos(\omega^h T)}{\omega^h} v_2^h + \frac{T^2}{2} d_1^h \\ \cos(\omega^h T) v_1^h - \sin(\omega^h T) v_2^h + T d_1^h \\ p_2^h + \frac{1-\cos(\omega^h T)}{\omega^h} v_1^h + \frac{\sin(\omega^h T)}{\omega^h} v_2^h + \frac{T^2}{2} d_2^h \\ \sin(\omega^h T) v_1^h + \cos(\omega^h T) v_2^h + T d_2^h \\ \omega^h + T d_3^h \\ d_1^h \\ d_2^h \\ d_3^h \end{bmatrix}$$

$$G_d = \begin{bmatrix} \frac{T^2}{2} & 0 & 0 & 0 & 0 & 0 \\ T & 0 & 0 & 0 & 0 & 0 \\ 0 & \frac{T^2}{2} & 0 & 0 & 0 & 0 \\ 0 & T & 0 & 0 & 0 & 0 \\ 0 & 0 & 1 & 0 & 0 & 0 \\ 0 & 0 & 0 & T & 0 & 0 \\ 0 & 0 & 0 & 0 & T & 0 \\ 0 & 0 & 0 & 0 & 0 & T \end{bmatrix}$$

$$w_1 \sim \mathcal{N}(0, Q_d^1).$$

The equation of the uniform motion for the model mismatch estimation is represented as follows:

$$x_{d,k+1}^{h,2} = f_d^2 x_{d,k}^{h,2} + G_d w_{2,k}$$

$$f_d^2\left(x_{s,k}^{h,2}\right) = \begin{bmatrix} p_1^h + v_1^h T + \frac{T^2}{2} d_1^h \\ v_1^h + T d_1^h \\ p_2^h + v_2^h T + \frac{T^2}{2} d_2^h \\ v_2^h + T d_2^h \\ \omega^h + T d_3^h \\ d_1^h \\ d_2^h \\ d_3^h \end{bmatrix}$$

$$w_2 \sim \mathcal{N}(0, Q_d^2)$$

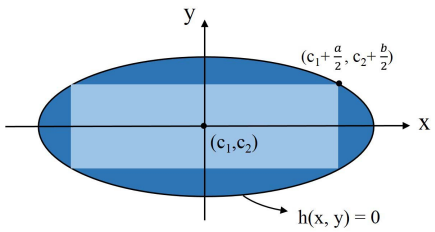

Fig. 12. Approximating the rectangle obstacle with an ellipse.

where $x_{d,k}^{h,i}$, $i = 1, 2$ represents the human motion state, including eight elements in the model mismatch estimation: p_1^h, v_1^h, p_2^h, v_2^h, ω^h, d_1^h, d_2^h, and d_3^h, where the first five states are defined as in Section III-B, and d_1^h, d_2^h, and d_3^h represent the model mismatch of longitudinal, lateral, and angular components, respectively; $w_{i,k}$, $i = 1, 2$ represents the process noise that follows a zero-mean Gaussian distribution with Q_d^i being the covariance matrix.

The observation model for the model mismatch estimation is represented as

$$y_{d,k}^h = C_d x_{d,k}^h + v_k \tag{9}$$

where $y_{d,k}^h$ denotes the observed human state at the time step k; v_k stands for measurement noise.

By using GPS or camera sensors, the human positions can be directly measured. Therefore, the parameters in observation model (9) are defined as

$$C_d = \begin{bmatrix} 1 & 0 & 0 & 0 & 0 & 0 & 0 & 0 \\ 0 & 0 & 1 & 0 & 0 & 0 & 0 & 0 \end{bmatrix}, \quad v \sim \mathcal{N}(0, V_d)$$

where V_d is the covariance matrix of the measurement noise.

B. Approximating Obstacles

Rectangular obstacles are approximated and analytically represented as ellipses. Let a and b be the length and width of a rectangular obstacle centered at the origin. Let (10) represent the ellipse that encloses the obstacle in the way that the four vertices of the rectangle lie on the boundary of the ellipse

$$\frac{x^2}{\alpha^2} + \frac{y^2}{\beta^2} = 1. \tag{10}$$

In addition, assume that the rectangle and ellipse have the same aspect ratio, which means $(a/b) = (\alpha/\beta)$, then by simple algebraic manipulation, we can obtain that $\alpha = (a/\sqrt{2})$ and $\beta = (b/\sqrt{2})$. Define $h(x, y) = 2(((x - c_1)^2)/a^2) + 2(((y - c_2)^2)/b^2) - 1$. The $h(x, y) = 0$ represent the shifted-center ellipse approximation of the rectangle with length a and width b. Any point (x, y) with $h(x, y) > 0$ lies outside the ellipse. Fig. 12 shows the schematic plot of the approximating ellipse for the rectangular obstacle centered at (c_1, c_2).

REFERENCES

[1] J. Casper and R. R. Murphy, "Human-robot interactions during the robot-assisted Urban search and rescue response at the World Trade Center," *IEEE Trans. Syst., Man, Cybern. B, Cybern.*, vol. 33, no. 3, pp. 367–385, Jun. 2003.

[2] S. Shen, N. Michael, and V. Kumar, "Autonomous multi-floor indoor navigation with a computationally constrained MAV," in *Proc. IEEE Int. Conf. Robot. Autom. (ICRA)*, May 2011, pp. 20–25.

[3] T. Ryan and H. J. Kim, "LMI-based gain synthesis for simple robust quadrotor control," *IEEE Trans. Autom. Sci. Eng.*, vol. 10, no. 4, pp. 1173–1178, Oct. 2013.
[4] V. Govindarajan, S. Bhattacharya, and V. Kumar, "Human-robot collaborative topological exploration for search and rescue applications," in *Distributed Autonomous Robotic Systems*. Springer, 2016, pp. 17–32.
[5] G. Kruijff *et al.*, "Designing intelligent robots for human-robot teaming in Urban search and rescue," in *Proc. AAAI Symp., Designing Intell. Robots*, 2012.
[6] J. Rios-Martinez, A. Spalanzani, and C. Laugier, "From proxemics theory to socially-aware navigation: A survey," *Int. J. Social Robot.*, vol. 7, no. 2, pp. 137–153, Apr. 2015.
[7] G. Ferrer, A. G. Zulueta, F. H. Cotarelo, and A. Sanfeliu, "Robot social-aware navigation framework to accompany people walking side-by-side," *Auto. Robots*, pp. 1–19, 2016.
[8] A. Cosgun, D. A. Florencio, and H. I. Christensen, "Autonomous person following for telepresence robots," in *Proc. IEEE Int. Conf. Robot. Autom. (ICRA)*, May 2013, pp. 4335–4342.
[9] T. Kruse, A. K. Pandey, R. Alami, and A. Kirsch, "Human-aware robot navigation: A survey," *Robot. Auto. Syst.*, vol. 61, no. 12, pp. 1726–1743, Dec. 2013.
[10] M. Svenstrup, T. Bak, and H. J. Andersen, "Trajectory planning for robots in dynamic human environments," in *Proc. IEEE/RSJ Int. Conf. Intell. Robots Syst. (IROS)*, Oct. 2010, pp. 4293–4298.
[11] J. R. Aiello, "Human spatial behavior," *Handbook Environ. Psychol.*, vol. 1, no. 1987, pp. 389–504, 1987.
[12] P. Henry, C. Vollmer, B. Ferris, and D. Fox, "Learning to navigate through crowded environments," in *Proc. IEEE Int. Conf. Robot. Autom. (ICRA)*, May 2010, pp. 981–986.
[13] D. Koller, J. Weber, and J. Malik, "Robust multiple car tracking with occlusion reasoning," in *Proc. Eur. Conf. Comput. Vis.*, May 1994, pp. 189–196.
[14] Y. Rui and Y. Chen, "Better proposal distributions: Object tracking using unscented particle filter," in *Proc. IEEE Comput. Soc. Conf. Comput. Vis. Pattern Recognit. (CVPR)*, vol. 2, Dec. 2001, pp. II-786–II-793.
[15] S. Yi, Z. He, X. You, and Y.-M. Cheung, "Single object tracking via robust combination of particle filter and sparse representation," *Signal Process.*, vol. 110, pp. 178–187, May 2015.
[16] C. Fulgenzi, C. Tay, A. Spalanzani, and C. Laugier, "Probabilistic navigation in dynamic environment using rapidly-exploring random trees and Gaussian processes," in *Proc. IEEE/RSJ Int. Conf. Intell. Robots Syst. (IROS)*, Sep. 2008, pp. 1056–1062.
[17] P. Trautman, J. Ma, R. M. Murray, and A. Krause, "Robot navigation in dense human crowds: Statistical models and experimental studies of human–robot cooperation," *Int. J. Robot. Res.*, vol. 34, no. 3, pp. 335–356, Mar. 2015.
[18] S. Xiao, Z. Wang, and J. Folkesson, "Unsupervised robot learning to predict person motion," in *Proc. IEEE Int. Conf. Robot. Autom. (ICRA)*, May 2015, pp. 691–696.
[19] J. K. Aggarwal and Q. Cai, "Human motion analysis: A review," *Comput. Vis. Image Understand.*, vol. 73, no. 3, pp. 428–440, Mar. 1999.
[20] B.-S. Yaakov, X. Li, and K. Thiagalingam, *Estimation With Applications to Tracking and Navigation: Theory Algorithms and Software*, vol. 245. New York, NY, USA: Wiley, 2001.
[21] D. Lee, C. Liu, and J. K. Hedrick, "Interacting multiple model-based human motion prediction for motion planning of companion robots," in *Proc. IEEE Int. Symp. Safety, Secur., Rescue Robot. (SSRR)*, Oct. 2015, pp. 1–7.
[22] C. E. García, D. M. Prett, and M. Morari, "Model predictive control: Theory and practice—A survey," *Automatica*, vol. 25, no. 3, pp. 335–348, May 1989.
[23] E. T. Hall *et al.*, "Proxemics [and comments and replies]," *Current Anthropol.*, vol. 9, nos. 2–3, pp. 83–108, Jun. 1968.
[24] R. Mead and M. J. Matarić, "Autonomous human–robot proxemics: Socially aware navigation based on interaction potential," *Auto. Robots*, pp. 1–13, 2016.
[25] D. S. Caveney, "Multiple model techniques in automotive estimation and control," Ph.D. dissertation, University of California, Berkeley, CA, USA, Tech. Rep. 31-46810 UMI, 2004.
[26] S. Haykin, *Kalman Filtering and Neural Networks*, vol. 47. Hoboken, NJ, USA: Wiley, 2004.
[27] S. Hong, T. Smith, F. Borrelli, and J. K. Hedrick, "Vehicle inertial parameter identification using extended and unscented Kalman filters," in *Proc. 16th Int. IEEE Conf. Intell. Transp. Syst. (ITSC)*, Oct. 2013, pp. 1436–1441.
[28] S. J. Julier and J. K. Uhlmann, "Unscented filtering and nonlinear estimation," *Proc. IEEE*, vol. 92, no. 3, pp. 401–422, Mar. 2004.
[29] V. A. Bavdekar, R. B. Gopaluni, and S. L. Shah, "Evaluation of adaptive extended Kalman filter algorithms for state estimation in presence of model-plant mismatch," in *Proc. 10th IFAC Int. Symp. Dyn. Control Process Syst.*, 2013, pp. 184–189.
[30] E. Wan and R. Van Der Merwe, "The unscented Kalman filter for nonlinear estimation," in *Proc. Adapt. Syst. Signal Process., Commun., Control Symp. (AS-SPCC)*, Oct. 2000, pp. 153–158.
[31] Z. Jiang, Y. He, and J. Han, "Disturbance estimation for RUAV using UKF with acceleration measurement," in *Proc. IEEE Int. Conf. Mechatron. Autom. (ICMA)*, Aug. 2015, pp. 500–505.
[32] J. J. Kuffner and S. M. LaValle, "RRT-connect: An efficient approach to single-query path planning," in *Proc. IEEE Int. Conf. Robot. Autom. (ICRA)*, vol. 2, Apr. 2000, pp. 995–1001.

Donghan Lee received the B.S. degree in mechanical engineering and the M.S. degree in automotive engineering from Hanyang University, Seoul, South Korea, in 2003 and 2006, respectively. He is currently pursuing the Ph.D. degree in mechanical engineering with the Vehicle Dynamics and Control Laboratory, University of California at Berkeley, Berkeley, CA, USA, headed by Prof. J. Karl Hedrick.

He was a Senior Research Engineer with Mando Corporation, Seongnam, South Korea. His current research interests include environment perceptions, human and vehicle motion predictions, and autonomous vehicle controls.

Chang Liu (S'15) received the B.S. degree in electrical engineering and the B.S. degree in applied mathematics from Peking University, Beijing, China, in 2011, and the M.S. degree in mechanical engineering and the M.S. degree in computer science from the University of California at Berkeley, Berkeley, CA, USA, in 2014 and 2016, respectively, where he is currently pursuing the Ph.D. degree in mechanical engineering with the Vehicle Dynamics and Control Laboratory, headed by Prof. J. Karl Hedrick.

His current research interests include path planning for robots and autonomous vehicles, distributed filtering for multiagent systems, and human-robot collaboration.

Yi-Wen Liao received the B.S. degree in mechanical engineering from National Taiwan University, Taipei, Taiwan, in 2010, and the M.S. degree in mechanical engineering from the University of Michigan, Ann Arbor, MI, USA, in 2012. She is currently pursuing the Ph.D. degree with the Department of Mechanical Engineering, Vehicle Dynamics and Control Laboratory, University of California at Berkeley, Berkeley, CA, USA, headed by Prof. J. Karl Hedrick.

Her current research interests include robust model predictive control, adaptive nonlinear control, vehicle dynamics, and their applications to autonomous driving systems.

J. Karl Hedrick received the B.S. degree in engineering mechanics from the University of Michigan, Ann Arbor, MI, USA, in 1966, and the M.S. and Ph.D. degrees in aeronautical and astronautical engineering from Stanford University, Stanford, CA, USA, in 1970 and 1971, respectively.

He is currently the James Marshall Wells Professor of Mechanical Engineering with the Department of Mechanical Engineering, University of California at Berkeley, Berkeley, CA. His current research interests include nonlinear control and its application to transportation systems.